Correspondence to:
X. Chu and W. Fong,
Xinzhao.Chu@Colorado.EDU;
Weichun.Fong@Colorado.EDU

Lidar and CTIPe model studies of the fast amplitude growth with altitude of the diurnal temperature "tides" in the Antarctic winter lower thermosphere and dependence on geomagnetic activity

Weichun Fong[1,2], **Xinzhao Chu**[1,2], **Xian Lu**[1], **Cao Chen**[1,2], **Timothy J. Fuller-Rowell**[1,3], **Mihail Codrescu**[3], and **Arthur D. Richmond**[4]

[1]Cooperative Institute for Research in Environmental Sciences, University of Colorado Boulder, Boulder, Colorado, USA, [2]Department of Aerospace Engineering Sciences, University of Colorado Boulder, Boulder, Colorado, USA, [3]Space Weather Prediction Center, NOAA, Boulder, Colorado, USA, [4]High Altitude Observatory, National Center for Atmospheric Research, Boulder, Colorado, USA

Abstract Four years of lidar observations at McMurdo reveal that the fast amplitude growth with altitude of diurnal temperature tides from 100 to 110 km during Antarctic winters, exceeding that of the freely propagating tides from the lower atmosphere, increases in strength with the *Kp* magnetic activity index. Simulations with the Coupled Thermosphere Ionosphere Plasmasphere Electrodynamics (CTIPe) model reproduce the lidar observations and exhibit concentric ring structures of diurnal amplitudes encircling the south geomagnetic pole and overlapping the auroral zone. These findings point to a magnetospheric source origin. Mechanistic studies using CTIPe show that the adiabatic cooling/heating associated with Hall ion drag is the dominant source of this feature, while Joule heating is a minor contributor due to the counteraction by Joule-heating-induced adiabatic cooling. The sum of total dynamical effects and Joule heating explains ~80% of the diurnal amplitudes. Auroral particle heating, lower atmosphere tides, and direct solar heating have minor contributions.

1. Introduction

Two years of lidar observations at McMurdo (77.8°S, 166.7°E) have revealed a superexponential amplitude growth with altitude of diurnal temperature tides in the lower thermosphere from 100 to 110 km during Antarctic winters in 2011 and 2012, exceeding that of the freely propagating tides originating from the lower atmosphere [*Fong et al.*, 2014, Figure 5]. Such fast growth exists for all levels of the *Kp* magnetic activity index, with larger *Kp* corresponding to larger tidal amplitudes and faster growth rates with altitude, indicating a connection with geomagnetic activity and the strengths of the magnetospheric sources. The slopes of tidal phases become steeper above 100 km, and the tidal phases barely change with altitude from 100 to 106 km, although the phases turn to be downward above 106 km. Such phase structure changes and *Kp* dependence suggest additional tidal sources near or above 100 km. Besides solar and chemical heating, the consequences of magnetospheric sources must be considered at polar latitudes.

Numerical simulations have revealed that magnetospheric forcing can enhance thermospheric tides at high latitudes [*Fuller-Rowell et al.*, 1991; *Fesen et al.*, 1993; *Fesen*, 1997; *Müller-Wodarg et al.*, 2001]. The effects of magnetospheric convection can be transferred to the horizontal neutral wind through ion drag [*Zhu et al.*, 2005], causing rotation and convergence/divergence of the airflow. The convergent/divergent horizontal winds induce vertical winds because of the requirement of mass continuity and result in adiabatic cooling/heating [*Kwak and Richmond*, 2007, 2014]. Joule heating can also induce vertical motion, and the resultant dynamical cooling/heating tends to counteract the Joule-heating-induced temperature changes. The ion drag causes a change of the bulk motion (wind) kinetic energy and has a momentum contribution from both the Pedersen conductivity (Pedersen drag) and the Hall conductivity (Hall drag). Pedersen drag is perpendicular to the electric field and tends to be rotational; Hall drag is parallel to the electric field, so it tends to be divergent or convergent [*Richmond*, 1995]. Auroral activity enhances particle precipitation heating via increased energetic particle fluxes. It also enhances Joule heating and both components of ion drag via increased conductivity. All of these mechanisms contribute to the lower thermosphere energetics

and cause the change of internal energy (temperature). The magnetospheric sources vary with magnetic local time, in addition to having irregular variations, and contribute to the in situ generation of diurnal tides.

Despite such a general understanding, it is still unknown at which altitudes the different heating mechanisms can act as tidal sources near McMurdo. The enhanced temperature tides indicate a manifestation of ion-neutral coupling and magnetospheric energy dissipation in the lower thermosphere. In this work, we attempt to quantify the relative contributions of the range of potential mechanisms of in situ tidal generation in the lower thermosphere using the Coupled Thermosphere Ionosphere Plasmasphere Electrodynamics (CTIPe) model [*Fuller-Rowell et al.*, 2002]. The main questions to answer include the following: What mechanisms are responsible for the observed diurnal tide enhancement? How does geomagnetic activity affect the energetics in the lower thermosphere? The model simulations will be compared to the new lidar observations spanning 4 years from 2011 to 2014 at McMurdo. Concerning the designation of the 24 h component of the temperature variation as a "tide," we followed the practice of some previous authors [e.g., *Fesen*, 1997] to designate as a tide any periodic variation of the atmosphere that is a harmonic of 1 day, regardless of the source.

2. Updated Lidar Observations and CTIPe Model Simulations

McMurdo is located on Ross Island, near the poleward edge of auroral oval. Since the Fe Boltzmann lidar observations at McMurdo started in December 2010 [*Chu et al.*, 2011a, 2011b], 4 years of temperature data (30–110 km) have been acquired so far. The ~530 h of data collected in the last two winters (May through August in 2013 and 2014) are more extensive than those in the first two winters (~330 h in 2011 and 2012). We analyze the new data sets to confirm the fast growth findings that were based on the first two winters of data [*Fong et al.*, 2014]. As illustrated in Figures 1a and 1b, the latter 2 years of data support the original findings of fast growth in diurnal tidal amplitudes and changing phase structures but give somewhat smaller amplitudes than the earlier 2 years. This is likely due to the smaller average Kp index during the observations, as the average Kp indices are 1.95 and 1.71 for 2011–2012 and 2013–2014, respectively, during the lidar observations.

The CTIPe model is a global, time-dependent, and self-consistent upper atmosphere model, which solves equations of momentum, energy, and continuity for neutrals and ions on an Eulerian corotating spherical grid [*Fuller-Rowell et al.*, 2002]. It has evolved over the past few decades and currently consists of four distinct components that run concurrently and are fully coupled. The neutral atmosphere is solved with resolutions of 18° in longitude and 2° in latitude, and each longitude slice sweeps through local time with a 1 min time step. For the vertical direction, it uses a pressure-based coordinate system of 15 levels at one-scale-height steps, starting from the lower boundary of 1 Pa at ~80 km. The model requires several external drivers, such as tidal inputs at the lower boundary, solar UV and EUV, and magnetospheric sources. More detailed descriptions of the model can be found in *Fuller-Rowell et al.* [2002] and *Maruyama et al.* [2007].

In this study, three different model runs from May to August in 2011 and 2012 were launched. The first one is a real-time run, for which the aforementioned external drivers are fed to the model based on real observations, the second is a run with Hall drag turned off, and the third is a run with the lower boundary tidal inputs from Global Scale Wave Model (GSWM) [*Hagan and Forbes*, 2002, 2003; *Zhang et al.*, 2010a, 2010b] turned off in order to investigate the effects from the lower atmosphere. A diurnal temperature composite is formed with the real-time model run output of two Antarctic winters using the same procedure as described in *Fong et al.* [2014]. The diurnal temperature tides are then derived from the composite with the same harmonic fitting as in *Fong et al.* [2014]. The model results from 80 to 200 km near McMurdo are compared with the 4 years of 80–110 km lidar observations in Figures 1c and 1d. It is clear that the CTIPe diurnal tidal amplitudes have similar behaviors as the lidar observations from 80 to 110 km, including that of the amplitudes being small below 100 km and increasing rapidly with altitude above 100 km from a few kelvin to over 20 K. The phase structures of CTIPe between 100 and 110 km are also comparable to the lidar observations (difference within 2–5 h). The good agreement between CTIPe and lidar results enables us to analyze the model results to determine the mechanisms behind the observed fast growth of the diurnal tide at high latitudes.

When such tidal analyses are applied to every model grid point, the resultant diurnal tidal amplitudes in the southern polar plots reveal a concentric ring surrounding the geomagnetic South Pole. An example of the temperature diurnal tidal amplitudes of the Antarctic region under different Kp conditions at pressure level 7
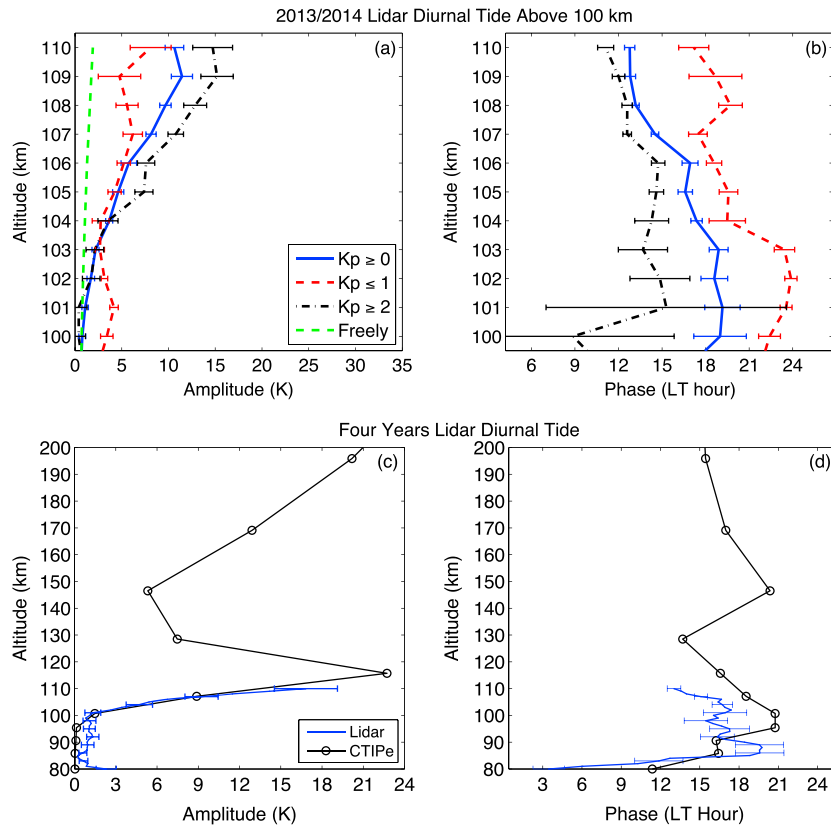
Figure 1. Lidar observations of diurnal temperature tides in the mesosphere and lower thermosphere region from 100 to 110 km during the winter season (May through August) at McMurdo, Antarctica: (a) the tidal amplitudes and (b) phases from 2013 to 2014 lidar data. (c) The tidal amplitude and (d) phase derived from 4 years of lidar observation (2011–2014) compared with the CTIPe modeled diurnal tidal amplitude and phase near McMurdo derived from the 8 month simulations (May through August in 2011 and 2012).

(~116 km) is shown in Figure 2. Note that level 7 corresponds to the altitude of the largest tidal amplitude in Figure 1c. Other adjacent levels show similar patterns as level 7 but with smaller amplitudes. To minimize the effect of direct solar heating, only June data in 2011 are used to derive tides all over the Antarctic region. We consider $Kp \geq 3$ as disturbed geomagnetic conditions and $Kp \leq 1$ as quiet conditions. It is obvious that the tidal amplitudes are larger under the disturbed conditions compared with quiet conditions, consistent with the lidar observations at lower altitudes. The tidal amplitudes form a concentric pattern that encircles the geomagnetic pole (white cross in Figure 2). The peak amplitudes averaged along the concentric patterns are about 20.3 K, 29.1 K, and 47.6 K and for $Kp \leq 1$, $Kp \geq 0$ (i.e., all Kp), and $Kp \geq 3$, respectively. The sizes of concentric patterns are similar for all the Kp conditions, and the distance from the geomagnetic pole to the amplitude peak is ~2000 km, corresponding to the geomagnetic latitude of ~72°S. Such concentric rings well overlap the observed auroral zones (http://legacy-www.swpc.noaa.gov/pmap/index.html), which strongly indicates a geomagnetic source of the tidal enhancements that will be studied below.

3. Mechanistic Studies

Treating the upper atmosphere as an ideal gas, we obtain from the entropy equation (note that the horizontal gradients of temperature and pressure are ignored) the heating rate:

$$c_P \frac{\partial T}{\partial t} = Q_{\text{diabatic}} - \left[c_P w \frac{\partial T}{\partial z} - \frac{w}{\rho} \frac{\partial p}{\partial z} - \frac{1}{\rho} \frac{\partial p}{\partial t} \right] \tag{1}$$

where T is the temperature, p is the pressure, c_P is the specific heat per unit mass at constant pressure, w is the vertical wind velocity with positive being upward, ρ is the density, t is the time, and z is the altitude. The first
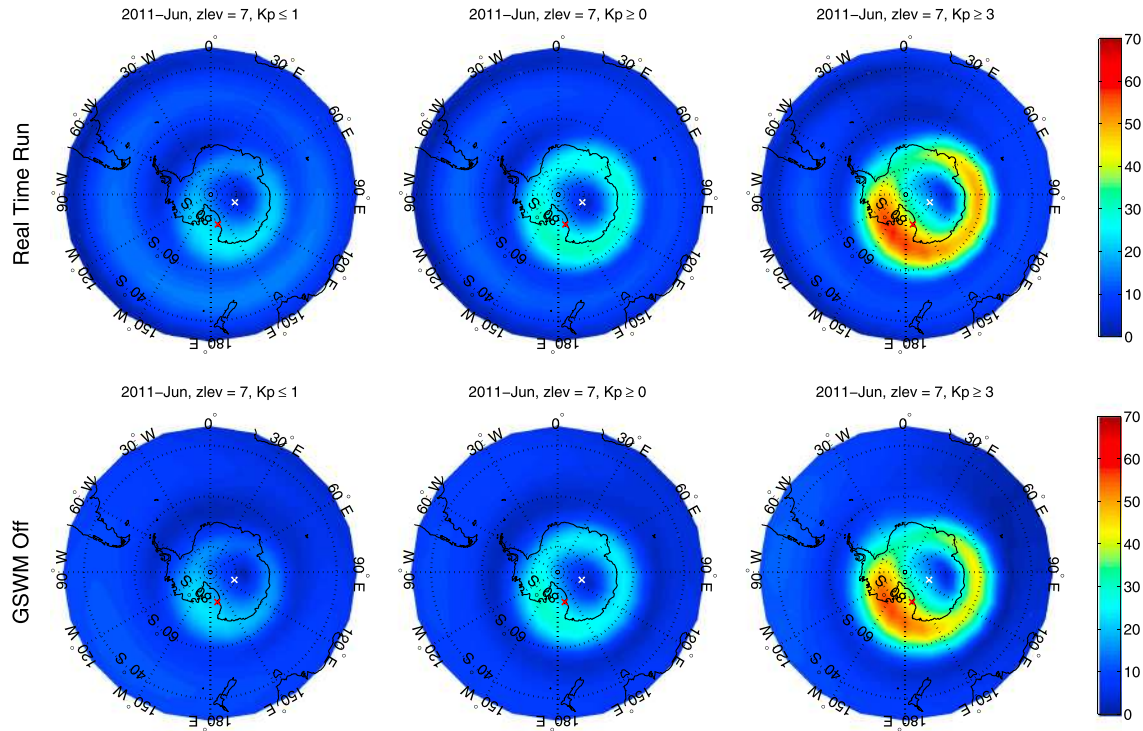
Figure 2. Diurnal tidal amplitudes of temperatures (unit: K) from the CTIPe simulations at pressure level 7 (~116 km) under different *Kp* conditions: (left) $Kp \leq 1$, (middle) $Kp \geq 0$, and (right) $Kp \geq 3$. In the top row are the real-time run cases, and in the bottom row are the cases with lower boundary tidal forcing removed. The location of the south geomagnetic pole is marked with a white cross and that of McMurdo with a red cross.

term on the right-hand side is the diabatic heating rate per unit mass due to heat transfer, i.e., all nonadiabatic processes (solar heating, chemical heating, Joule heating, auroral particle heating, vertical heat conduction, viscous heating, etc.), while the second term (in brackets) represents the adiabatic effects of vertical heat advection and work done to the surroundings of the air parcel in consideration. Among the diabatic terms, the Joule heating rate, which has been written out from the CTIPe model, is computed as $Q_{Joule} = \vec{J} \cdot \left(\vec{E} + \vec{V} \times \vec{B} \right)/\rho$, where $\vec{E}$ is the electric field computed from the electric potential provided by the empirical model Weimer 2005 [*Weimer*, 2005], $\vec{J}$ is the current density, $\vec{V}$ is the neutral wind velocity, and $\vec{B}$ is the geomagnetic field. To compute the adiabatic heating rate, we assume hydrostatic equilibrium so that $\partial p/\partial z = -\rho g$, where g is the gravitational acceleration, and take $\partial p/\partial t = 0$; thus, the adiabatic term becomes $\left[c_P w \frac{\partial T}{\partial z} + wg \right]$. Taking the vertical wind, temperature, and geopotential height output from CTIPe, the adiabatic heating rate is calculated using this simplified equation.

The diurnal tides induced by each of the above heating terms are then derived as follows. Equation (2) is fitted to the time series of the heating rate induced by each heating term, divided by c_p, so that the amplitudes and phases of the diurnal and semidiurnal tides are derived at every model grid point in the southern polar region.

$$\left(\frac{\partial T}{\partial t} \right)_{term} = A_{24}\omega_{24}\sin(\omega_{24}t + \varphi_{24}) + A_{12}\omega_{12}\sin(\omega_{12}t + \varphi_{12}) \qquad (2)$$

where A_{24} and A_{12} are the amplitudes, ω_{24} and ω_{12} are the angular frequencies, and φ_{24} and φ_{12} are the phases of diurnal and semidiurnal tides, respectively, associated with this heating term. Here the heating rate time series is obtained by the same diurnal composite method as used in Figure 2.

Figure 3 shows the diurnal temperature tidal amplitudes induced by Joule heating (Figures 3a–3c) and adiabatic heating (Figures 3d–3f) under different *Kp* conditions at CTIPe pressure level 7. The concentric ring patterns occur in all panels. The tidal amplitudes induced by the total effects of Joule heating and adiabatic heating (Figures 3g–3i) arithmetically averaged between 60°S and 90°S are 23.6 K, 14.5 K, and 11.4 K for $Kp \geq 3$, $Kp \geq 0$, and $Kp \leq 1$ conditions, respectively. These amplitudes make up about 80% of the corresponding
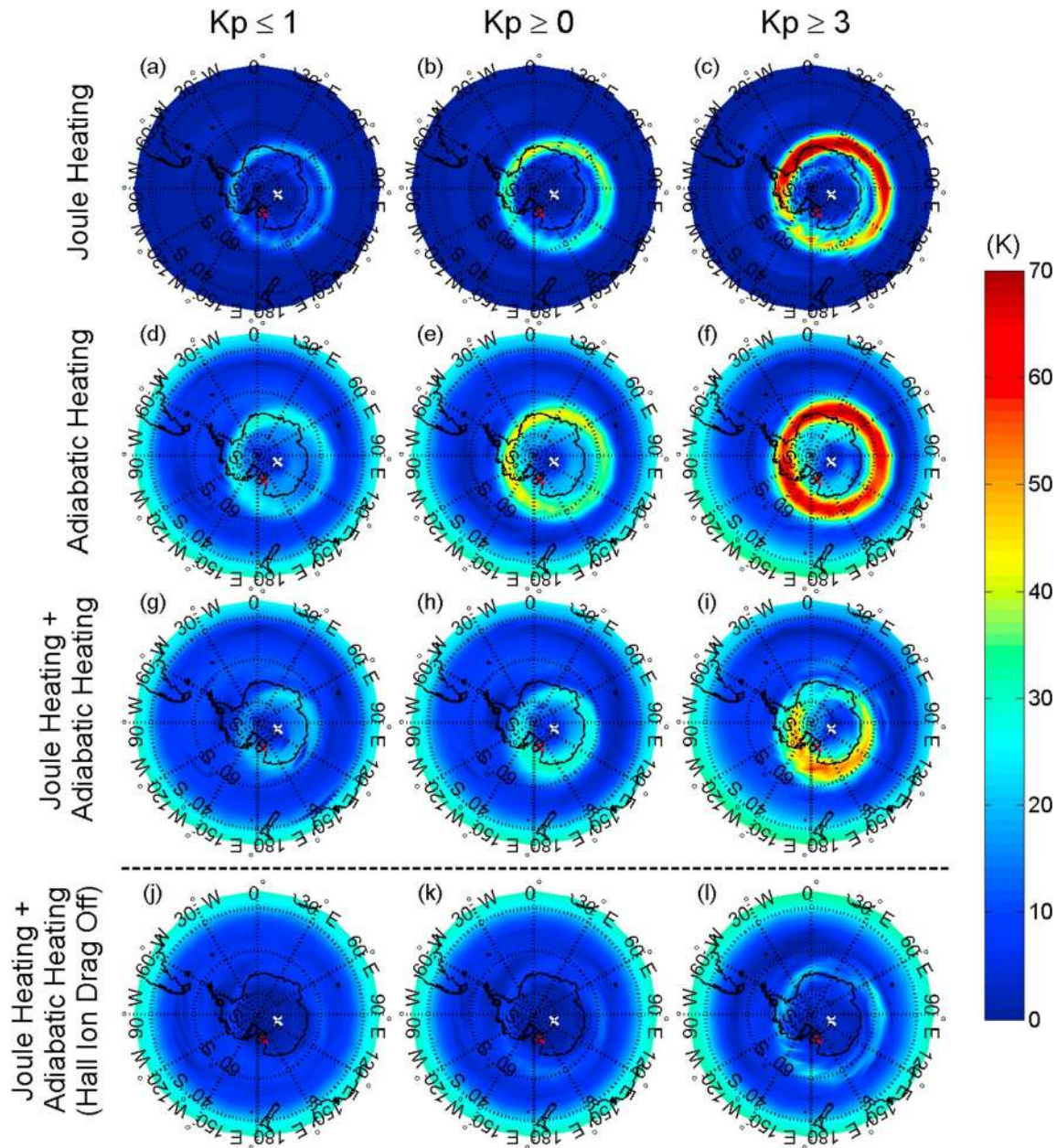
Figure 3. Real-time CTIPe model simulations in June 2011 on the diurnal tidal amplitudes of temperatures induced by individual heating terms: (a–c) Joule heating, (d–f) adiabatic heating, and (g–i) the sum of Joule heating and adiabatic heating. (j–l) The diurnal tidal amplitudes of temperatures when the Hall ion drag is removed from the CTIPe model. The simulation results are for CTIPe pressure level 7 (~116 km) under different magnetic activity indices of (left) $Kp \leq 1$, (middle) $Kp \geq 0$, and (right) $Kp \geq 3$, respectively.

simulated temperature tidal amplitudes (Figure 2), which are 29.5 K, 17.5 K, and 19.1 K for $Kp \geq 3$, $Kp \geq 0$, and $Kp \leq 1$ conditions, respectively. The particle precipitation heating makes only minor contributions to the diurnal tides below 120 km, according to the CTIPe simulation results (not shown): only 1–2 K even under disturbed conditions ($Kp \geq 3$), which are significantly smaller than that of the Joule heating or adiabatic heating at the same levels.

As pointed out in *Roble et al.* [1982], both ion-drag-induced convergent/divergent airflow and Joule heating can induce vertical motion, leading to the adiabatic heating/cooling. It is necessary to identify the dominant mechanism between the two. Considering that the Hall ion drag tends to dominate over the Pedersen ion drag below 120 km [*Kwak and Richmond*, 2007], a test run was launched with the Hall-ion-drag force removed
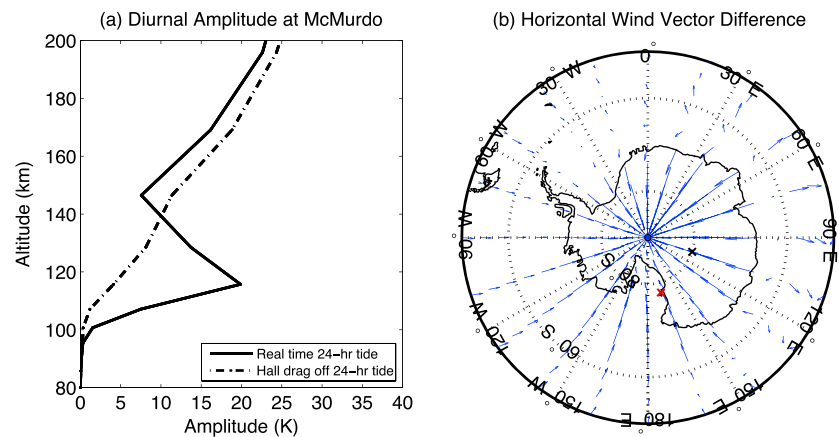
Figure 4. (a) Diurnal temperature amplitudes derived from the CTIPe real-time run and the Hall-drag-off run in June 2011. (b) Horizontal wind vector difference between the real-time run and the run without Hall ion drag at 116 km on 5 June 2011 at 06:00 UT.

from the momentum equations in the CTIPe model. The results are shown in Figures 3j–3l and Figure 4. Once the Hall ion drag is removed, the patterns of the induced diurnal tidal amplitudes (Figures 3j–3l) become very small compared with the real-time run (Figures 3g–3i), demonstrating that the adiabatic effects driven by Joule heating alone tend to cancel the Joule heating effects. This test also indicates that it is the adiabatic effects of the Hall ion drag that dominate the diurnal tidal forcing in Figures 3g–3i, which would explain the fact that the maximum amplitudes (Figures 3g–3i) occur at higher latitudes than the Joule heating effects (Figures 3a–3c). Taking McMurdo as an example, the induced diurnal amplitudes between 100 and 116 km are significantly reduced by ~80% at 116 km and ~85% at 106 km when compared with the real-time run case (Figure 4a). The horizontal winds in the case of the Hall-drag-off run are smaller than those of the real-time run (not shown), and the wind vector differences between the two runs show divergent and convergent patterns as illustrated in Figure 4b, instead of rotational patterns typical for Pedersen drag. Since Hall drag is in the direction of the electric field, the divergent and convergent patterns of the horizontal wind difference indicate the Hall drag dominance over Pedersen drag in the lower thermosphere below 120 km. The Hall drag tends to be offset by a counteracting horizontal pressure gradient force, so that it tends to produce increased pressure where the electric field is convergent and decreased pressure where the field is divergent. The convergence and divergence of the electric field maximize around the poleward edge of the auroral oval, near the polar cap boundary. Below 120 km, the amplitude of relative pressure perturbation grows with height, implying a diurnal variation of the scale height and temperature. Therefore, Hall drag tends to produce a diurnal temperature tide that maximizes around the polar cap boundary instead of at the center of the auroral zone, where Joule heating maximizes.

The simulation results also demonstrate the Kp dependence of the induced diurnal tidal amplitudes as well as the individual terms of adiabatic, Joule, and particle heating. Because the ion drag forcing is larger under more disturbed conditions due to the increased conductivities and electric field, and the Hall-ion-drag-induced adiabatic effect is the dominant source of diurnal tides as shown above, the aurora-enhanced ion drag induces stronger vertical motion, thus stronger adiabatic heating/cooling at larger Kp. Again, since the magnetospheric sources vary with magnetic local time, ion-drag-induced adiabatic effects have projections on the diurnal variations, contributing to the in situ generation of diurnal temperature tides and inducing the Kp dependence of the tidal amplitudes. The aurorally driven tides tend to be largest in the generation region and do not show much, if any, vertical propagation.

The contributions of the tides propagating from the lower atmosphere to the thermospheric tides are small in the polar region but significant in the midlatitudes, according to the CTIPe model run with lower boundary tidal forcing excluded (Figure 2, bottom row). The reduction of the diurnal tidal amplitude at McMurdo is only 0.7 K (relative change ~3.4%) when compared to the real-time run for the $Kp \geq 0$ case. It can also be seen that the lower boundary tidal forcing has greater impact (~65%) on the tidal amplitudes equatorward of 60° than on those of the polar regions (~10%), which indicates that the lower atmosphere tide is a dominant source in the

midlatitude and low-latitude regions. It should be noted that the GSWM tides used in the CTIPe model do not include all the tidal sources, such as nonlinear interactions between planetary waves and tides [*Zhang et al.*, 2010a, 2010b], and it is known that GSWM may underestimate the tidal amplitudes in the polar region [e.g., *Murphy et al.*, 2006; *Lübken et al.*, 2011].

We also investigate the contributions from direct solar heating, for which CTIPe shows that the induced diurnal amplitudes are less than 3 K poleward of 60°S and below 126 km near winter solstice. This is considered as a minor effect in this study. Another possible tidal source is chemical heating. Exothermic chemical processes could be enhanced due to particle precipitation; e.g., the dissociative ionization of O_2 could increase the concentration of atomic O and thus enhance the three-body reaction of atomic O: $O + O + M \rightarrow O_2 + M$, which is the dominant reaction above 100 km [*Smith et al.*, 2003]. However, according to *Smith et al.* [2003], although the heating rate of this three-body reaction can reach about ~12 K/d around 103 km, it does not have a pronounced diurnal cycle due to the long lifetime of O, which should also lead to a minor contribution to the temperature diurnal amplitude in the lower thermosphere.

4. Conclusions

After *Fong et al.* [2014] first reported the superexponential increase of the diurnal tidal amplitude in temperature from 100 to 110 km at McMurdo, the lidar observations in the winters of 2013 and 2014 confirm the fast growth with altitude of the diurnal tides and confirm that the tidal amplitudes increase in strength with the *Kp* index. The winter temperature tides simulated by the CTIPe model are consistent with the 4 years of lidar observations at McMurdo, and the fast growth features are nicely reproduced with clear *Kp* dependence. From the mechanistic studies using CTIPe, we conclude that the Hall-ion-drag-induced adiabatic effects, varying with magnetic local time, are the dominant source responsible for the observed diurnal tides at McMurdo. Although the Joule heating term alone is large, it has a minor contribution to the diurnal tides due to the counteraction by Joule-heating-induced adiabatic effects. CTIPe simulations predict that such diurnal temperature amplitudes in situ generated by polar ionospheric convection in the lower thermosphere maximize near the polar cap boundary and form concentric ring patterns that encircle the south geomagnetic pole. Aurora increases the Hall ion drag through increasing conductivities and electric field, leading to stronger vertical motion and adiabatic effects, which explains the *Kp* dependence of the observed diurnal tidal amplitudes. Other tidal sources, such as particle precipitation, tides propagating from the lower thermosphere, and direct solar heating, are shown to have minor effects on the observed diurnal tides in the lower thermosphere, according to the CTIPe model simulations. Lastly, it is worth to point out that the one-scale-height resolution of CTIPe is not ideal, but it is sufficient to simulate the in situ forcing-induced local dynamical response and the adiabatic consequences, through the physical processes captured in the model. There is an effort underway to improve the vertical resolution, at which point we expect to confirm the physics of the response, although the amplitudes of the temperature response may change.

References

Chu, X., W. Huang, W. Fong, Z. Yu, Z. Wang, J. A. Smith, and C. S. Gardner (2011a), First lidar observations of polar mesospheric clouds and Fe temperatures at McMurdo (77.8°S, 166.7°E), Antarctica, *Geophys. Res. Lett.*, *38*, L16810, doi:10.1029/2011GL048373.

Chu, X., Z. Yu, C. S. Gardner, C. Chen, and W. Fong (2011b), Lidar observations of neutral Fe layers and fast gravity waves in the thermosphere (110–155 km) at McMurdo (77.8°S, 166.7°E), Antarctica, *Geophys. Res. Lett.*, *38*, L23807, doi:10.1029/2011GL050016.

Fesen, C. G. (1997), Geomagnetic activity effects on thermospheric tides: A compendium of theoretical predictions, *J. Atmos. Sol. Terr. Phys.*, *59*(7), 785–803.

Fesen, C. G., A. D. Richmond, and R. G. Roble (1993), Theoretical effects of geomagnetic activity on thermospheric tides, *J. Geophys. Res.*, *98*(A9), 15,599–15,612, doi:10.1029/93JA01188.

Fong, W., X. Lu, X. Chu, T. J. Fuller-Rowell, Z. Yu, B. R. Roberts, C. Chen, C. S. Gardner, and A. J. McDonald (2014), Winter temperature tides from 30 to 110 km at McMurdo (77.8°S, 166.7°E), Antarctica: Lidar observations and comparisons with WAM, *J. Geophys. Res. Atmos.*, *119*, 2846–2863, doi:10.1002/2013JD020784.

Fuller-Rowell, T. J., D. Rees, H. F. Parish, T. S. Virdi, P. J. S. Williams, and R. M. Johnson (1991), Lower thermosphere coupling study: Comparison of observations with predictions of the University College London-Sheffield thermosphere-ionosphere model, *J. Geophys. Res.*, *96*(A2), 1181–1202, doi:10.1029/90JA02315.

Fuller-Rowell, T. J., G. H. Millward, A. D. Richmond, and M. V. Codrescu (2002), Storm-time changes in the upper atmosphere at low latitudes, *J. Atmos. Sol. Terr. Phys.*, *64*, 1383–1391, doi:10.1016/S1364-6826(02)00101-3.

Hagan, M. E., and J. M. Forbes (2002), Migrating and nonmigrating diurnal tides in the middle and upper atmosphere excited by tropospheric latent heat release, *J. Geophys. Res.*, *107*(D24), 4754, doi:10.1029/2001JD001236.

Hagan, M. E., and J. M. Forbes (2003), Migrating and nonmigrating semidiurnal tides in the middle and upper atmosphere excited by tropospheric latent heat release, *J. Geophys. Res.*, *108*(A2), 1062, doi:10.1029/2002JA009466.

Kwak, Y.-S., and A. D. Richmond (2007), An analysis of the momentum forcing in the high-latitude lower thermosphere, *J. Geophys. Res., 112*, A01306, doi:10.1029/2006JA011910.

Kwak, Y.-S., and A. D. Richmond (2014), Dependence of the high-latitude lower thermospheric wind vertical vorticity and horizontal divergence on the interplanetary magnetic field, *J. Geophys. Res. Space Physics, 119*, 1356–1368, doi:10.1002/2013JA019589.

Lübken, F.-J., J. Höffner, T. P. Viehl, B. Kaifler, and R. J. Morris (2011), First measurements of thermal tides in the summer mesopause region at Antarctic latitudes, *Geophys. Res. Lett., 38*, L24806, doi:10.1029/2011GL050045.

Maruyama, N., et al. (2007), Modeling storm-time electrodynamics of the low-latitude ionosphere-thermosphere system: Can long lasting disturbance electric fields be accounted for?, *J. Atmos. Sol. Terr. Phys., 69*, 1182–1199.

Müller-Wodarg, I. C. F., A. D. Aylward, and T. J. Fuller-Rowell (2001), Tidal oscillations in the thermosphere: A theoretical investigation of their sources, *J. Atmos. Sol. Terr. Phys., 63*, 899–914.

Murphy, D. J., et al. (2006), A climatology of tides in the Antarctic mesosphere and lower thermosphere, *J. Geophys. Res., 111*, D23104, doi:10.1029/2005JD006803.

Richmond, A. D. (1995), Ionospheric electrodynamics, in *Handbook Of Atmospheric Electrodynamics*, vol. II, edited by H. Volland, pp. 249–290, CRC Press, Boca Raton, Fla.

Roble, R. G., R. E. Dickinson, and E. C. Ridley (1982), Global circulation and temperature structure of thermosphere with high-latitude plasma convection, *J. Geophys. Res., 87*(A3), 1599–1614, doi:10.1029/JA087iA03p01599.

Smith, A. K., D. R. Marsh, and A. C. Szymczak (2003), Interaction of chemical heating and the diurnal tide in the mesosphere, *J. Geophys. Res., 108*(D5), 4164, doi:10.1029/2002JD002664.

Weimer, D. R. (2005), Improved ionospheric electrodynamic models and application to calculating Joule heating rates, *J. Geophys. Res., 110*, A05306, doi:10.1029/2004JA010884.

Zhang, X., J. M. Forbes, and M. E. Hagan (2010a), Longitudinal variation of tides in the MLT region: 1. Tides driven by tropospheric net radiative heating, *J. Geophys. Res., 115*, A06316, doi:10.1029/2009JA014897.

Zhang, X., J. M. Forbes, and M. E. Hagan (2010b), Longitudinal variation of tides in the MLT region: 2. Relative effects of solar radiative and latent heating, *J. Geophys. Res., 115*, A06317, doi:10.1029/2009JA014898.

Zhu, X., E. R. Talaat, J. B. H. Baker, and J.-H. Yee (2005), A self-consistent derivation of ion drag and Joule heating for atmospheric dynamics in the thermosphere, *Ann. Geophys., 23*, 3313–3322, doi:10.5194/angeo-23-3313-2005.